remote sensing

MDPI

Article

A Study on Remote Monitoring of NO_x Emissions from Inland Vessels

Mengtao Deng [1,*], Jianbo Hu [2], Zhaoyu Qi [2] and Shitao Peng [2]

[1] Key Laboratory of Environmental Protection Technology on Water Transport, Tianjin Research Institute for Water Transport Engineering, M.O.T., Tianjin 300456, China
[2] National Engineering Research Center of Port Hydraulic Construction Technology, Tianjin Research Institute for Water Transport Engineering, M.O.T., Tianjin 300456, China; hujb@tiwte.ac.cn (J.H.); qizhy@tiwte.ac.cn (Z.Q.); pengshitao@tiwte.ac.cn (S.P.)
* Correspondence: dengmt@tiwte.ac.cn

Abstract: In order to demonstrate the feasibility of the tunable diode laser absorption spectroscopy (TDLAS) technology for monitoring NO_x emissions from inland vessels, an equipment is designed to monitor emissions for inland vessels. The equipment was installed at the Jianbi locks, where experimental measurements were conducted on vessels passing through the locks, with a total of 330 vessels being measured. The detection rate for vessels was 50.3%, with a detection rate of 72.4% for fully loaded vessels and 24.7% for unloaded vessels. In addition, the exhaust emission patterns of inland vessels, the NO_x emission patterns and detection rate of fully loaded and unloaded vessels, and the key parameter of the NO_x emission factor of inland vessels were comprehensively analyzed. The experimental results show that CO_2 and NO_x in the exhaust gas of inland vessels have high signal intensity and good synchronization and can be applied to the regulatory monitoring of NO_x emissions from inland vessels. Furthermore, the ratios of NO/CO_2 and NO_2/CO_2 from fully loaded and unloaded vessels were significantly different. indicating that the NO_2 indicator must be included in the remote monitoring indicators for inland vessel exhaust gases. Otherwise, the remote monitoring results for NO_x may be significantly underestimated.

Keywords: TDLAS; inland vessel; NO_x; detection rate; emission patterns

Academic Editor: Carmine Serio

Received: 8 November 2024
Revised: 23 December 2024
Accepted: 3 January 2025
Published: 6 January 2025

Citation: Deng, M.; Hu, J.; Qi, Z.; Peng, S. A Study on Remote Monitoring of NO_x Emissions from Inland Vessels. *Remote Sens.* **2025**, *17*, 168. https://doi.org/10.3390/rs17010168

1. Introduction

Shipping is an important part of the global economy, accounting for 80–90% of world trade transportation, but air pollution caused by ships has long been overlooked [1,2]. Studies have shown that emissions of CO_2, SO_2, and NO_x from ships account for 2.7%, 4~9%, and 15%, respectively, of all human emissions [3,4]. The major port cities in the Yangtze River Delta and the Pearl River Delta in China have seen shipping become one of the main sources of local air pollution. Pollutants emitted by ships play a significant role in air quality, human health, and climate [5–7]. They not only affect the air quality of coastal areas but also impact regions hundreds of kilometers away from the emission sources [8]. Port cities are most affected by ship pollution, followed by cities along rivers. In the shipping system, inland waterways, which are mostly near or flow through populated residential areas, have a greater impact on the public, and studies have shown that inland vessels are the main contributors to the impact of shipping on urban air quality, with 40–80% of $PM_{2.5}$ from shipping sources in Shanghai coming from inland vessels [9].

In 2018, there were 124,300 inland vessels in service in China, which is seven times the number of inland waterway vessels in Europe [10]. Overall, there is a huge potential for NO_x emission reduction from ships in China, and it is also an inevitable trend to improve air quality in coastal port cities in the future. With the continuous advancement of land-based NO_x emission control in China, the land-based NO_x emission reduction potential is becoming smaller and smaller, and the demand for NO_x emission control and regulation of inland vessels is becoming more and more urgent.

In the early 1980s, research on tunable diode laser absorption spectroscopy (TDLAS) technology was continuously conducted abroad. In 1991, K.R. Carduner and his team used TDLAS technology for researching the detection of automobile engines to judge whether the engine is working properly or not by the content of SO_2 in its exhaust gas, and the instrument can detect SO_2 gas from 0.1 to 1 ppm [11].

In 2008–2009, Daniel, an American academic, monitored CO, HC, and NO_x emissions from 307 inland vessels for the first use of a remote monitoring device at a lock (Hiram M. Chittenden Locks, Seattle). In 2009, the team also monitored NO_x emissions from nine passing vessels for the first time on a bridge (Lions Gate Bridge, Vancouver). The telemetry results were close to those of the laboratory tests, confirming the feasibility of using telemetry to regulate the exhaust emissions from inland vessels [12,13]

In 2012, Waclawek et al. developed a sensor platform. The platform uses a quantum cascade laser (QCL) with a center wavelength of 7.25 μm and is capable of detecting SO_2 at ppb concentration levels with a time response of 1 s at 20.5 °C, making it suitable for environmental and industrial monitoring [14]. In 2014, Hartmann et al. developed a sensor for breath detection based on TDLAS technology, which reduces optical fringing using a self-developed fringe suppression method and is capable of achieving CO_2 measurements with a concentration resolution of 300 ppm at 4 vol% [15]. In 2020, Genner et al. applied quantum cascade lasers for the detection of multi-component (CO, NO, NO_2, and SO_2) polluting hazardous gases, with a minimum detection limit of 1.4 ppb for SO_2 [16]. In 2020, the EU-funded SCIPPER project detects the ratio of SO_2 and CO_2 with the help of a 400 m optical range gas cell, thus enabling high-precision detection of the sulfur–carbon ratio of marine fuel oils, with gas measurements up to the ppt level [17].

The above research results are only exploratory attempts to prove the feasibility but have not been popularized and applied, probably because inland navigation in the United States is not developed or the routes are too dispersed. The application prospect is far less promising compared to China's Yangtze River, Xijiang River, the Beijing-Hangzhou Canal, and other densely navigable waterways.

China's research on TDLAS technology started late but developed rapidly. In 2015, Yao et al. from the Anhui Institute of Optics and Fine Mechanics, Chinese Academy of Sciences, developed a miniaturized CO_2 detection system using the direct absorption technique in TDLAS, which carried out ball-loaded measurements of CO_2 concentration profiles and obtained molecular number density distributions of CO_2 in the troposphere below 10 km [18].

In 2021, Liu et al. from Taiyuan University of Science and Technology (TUST) used TDLAS technology for the simultaneous detection of SO_2 and SO_3 in industrial exhaust gases based on a 7.16 μm QCL [19]. In 2022, Zhang et al. from Changchun Institute of Optics, Fine Mechanics and Physics, Chinese Academy of Sciences, designed a Zynq-based data acquisition system for CO_2 gas detection, which realized the acquisition and processing of gas concentration, pressure, and temperature signals [20].

China currently lacks research reports, inland ship exhaust telemetry technology, and related equipment, highlighting an urgent need for independent research and development. Drawing on the application scenario of remote sensing technology for motor vehicle

exhaust, due to the presence of approximately 400 ppm of carbon dioxide in the ambient air, the remote monitoring distance is usually not more than 30–50 m; otherwise, the exhaust signal may be submerged in higher concentration background processes. However, inland waterways are relatively narrow, especially in ship locks, which have the conditions for the application of ship exhaust telemetry technology. Therefore, there is an urgent need to carry out research on NO_x emission telemetry technology for inland vessels to fill the gap of NO_x emission supervision capability for inland vessels.

The rest of this paper is organized as follows. Section 1 contains a literature review of existing research on remote monitoring technologies for regulating ship exhaust emissions. On the basis of the studies carried out, there is a lack of research on the regulation of NO_x emissions from inland vessels. Section 2 analyzes the methodology and measurement system in detail. Section 3 focuses on the detailed analysis of the experimental results; based on the experimental results, the difficulties and challenges of applying TDLAS-based remote monitoring technology for inland vessel exhaust monitoring are discussed. Sections 4 and 5 presents the discussion and conclusions of this paper.

2. Materials and Methods

TDLAS technology is the abbreviation for tunable diode laser absorption spectroscopy [21,22]. According to the Lambert–Beer's Law [23,24], when a parallel beam of monochromatic light is transmitted perpendicularly through a gas, the gas absorbs light of a specific wavelength. This absorption causes energy attenuation, and the absorbance is directly proportional to the concentration of the absorbing substance and the thickness of the absorption layer [25].

Using a narrow linewidth (<2 MHz), a wavelength-tunable laser, an absorption line v_0 of the gas to be measured can be scanned to obtain a high-resolution, interference-free spectrum of an absorption feature of the gas to be measured.

When a light beam of intensity I_0 and frequency v passes through a section of a gaseous medium, the gas molecules absorb the photons and produce an energy level jump that attenuates the light intensity and transmits the light intensity I, defining the absorbance $A(v)$.

$$A(\nu - \nu_0) = \ln \frac{I_0(\nu - \nu_0)}{I(\nu - \nu_0)} = \int_0^L k_v(x)dx \quad (1)$$

where L [cm] is the optical path length through the gas medium, k_v [cm^{-1}] is the absorption coefficient, which represents the superposition of the absorptions of all gases at frequency v, and k_v is often specified in two ways:

$$k_v = \sum_{j=1}^{J} n_j \sum_{i=1}^{Ni} \sigma_{i,j} = \sum_{j=1}^{J} n_j \sum_{i=1}^{Ni} S'_{i,j}(T)\phi_{i,j}(\nu - \nu_0) \quad (2)$$

$$k_v = P \sum_{j=1}^{J} X_j \sum_{i=1}^{Ni} S_{i,j}(T)\phi_{i,j}(\nu - \nu_0) \quad (3)$$

Equation (2), n_j [molecule·cm^{-3}] represents the molecular number density of gas component j, $\sigma_{i,j}$ [cm^2] represents the absorption cross-section corresponding to transition i of the gas in component j. The unit of line intensity $S'_{i,j}(T)$ is $cm^{-1}/(\text{molecule}\cdot cm^{-2})$, and $\phi_{i,j}$ [cm] is the absorption line function. In Equation (3), P [atm] is the total gas pressure, X_j is the concentration of gas component j, expressed as a mole fraction or partial pressure ratio, PX_j is the partial pressure of component j, and $S_{i,j}$ [$cm^{-2}atm^{-1}$] and $\phi_{i,j}$ [cm] are the absorption line intensity and line shape at the time of the leap i of gas compo-

nent j, respectively. The two-line strength units can be converted according to the ideal gas theorem:

$$S\left[\mathrm{cm}^{-2}\mathrm{atm}^{-1}\right] = \frac{7.339 \times 10^{21}\left[\left(\mathrm{molecule}\cdot\mathrm{cm}^{-3}\cdot\mathrm{K}\right)/\mathrm{atm}\right] S'\left[\mathrm{cm}^{-1}/\left(\mathrm{molecule}\cdot\mathrm{cm}^{-2}\right)\right]}{T[\mathrm{K}]} \tag{4}$$

According to Equations (1) and (2), for a homogeneous gaseous medium, a certain absorption line frequency v, k_v independent of the optical path can be obtained:

$$A(\nu) = L \cdot k_v(x) = L \cdot N \cdot S'(T) \cdot \phi(\nu - \nu_0) \tag{5}$$

where $\phi(\nu)$ depends on the temperature and pressure of the measurement environment and needs to be obtained through complex theoretical calculations. In practice, the normalized definition of $\phi(\nu)$ to v can be used to integrate Equation (5):

$$\int_{-\infty}^{+\infty} A(\nu - \nu_0)d\nu = L \cdot N \cdot S'_{i,j}(T) \cdot \int_{-\infty}^{+\infty} \phi(\nu - \nu_0)d\nu = L \cdot N \cdot S'(T) \tag{6}$$

The molecular number density N [molecule·cm^{-3}] can be obtained after the absorbance $A(\nu)$, the absorption range L [cm], and the absorption line intensity $S'(T)$ [$\mathrm{cm}^{-1}/\left(\mathrm{molecule}\cdot\mathrm{cm}^{-2}\right)$] are known.

In practical applications, the spectral characteristics of molecular absorption can be obtained by direct absorption or wavelength modulation, which can be selected for different measurement occasions and measurement needs.

In this paper, a remote monitoring equipment based on TDLAS technology for inland vessel emissions is designed. As shown in Figure 1, the ship exhaust equipment controls 4 lasers at the same time, and using time-division multiplexing, the 4 lasers are sent out using time-sharing, which are converted into a single beam of light sent out through the internal merging optical path. The beam passes through the detection area and is reflected again through the angle mirror, passing through the area and returning to the equipment. The beam is output to the detector through the mirror, which detects the laser signals at different times and calculates the concentration of each gas in the area.

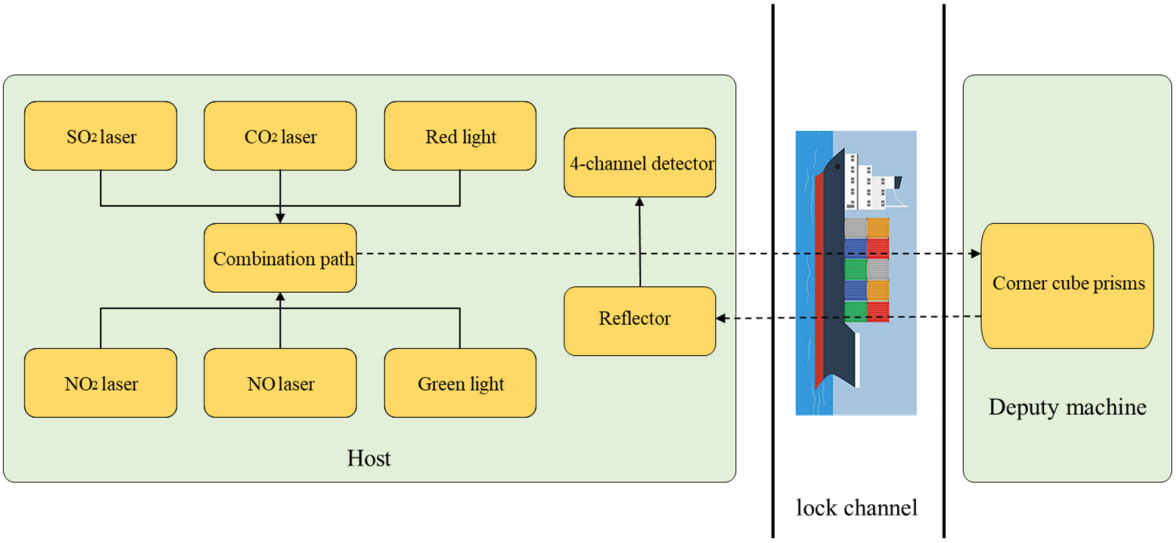

Figure 1. Schematic diagram of a ship exhaust telemetry system for NO_x regulation of inland vessels.

The system uses wavelength modulation spectroscopy, which was calibrated in the laboratory with standard gas before on-site testing. An adaptive concentration compen-

sation algorithm is used internally, eliminating the need for frequent equipment calibration. The wavelength and power of the laser are as follows: NO_2 (6.2 μm, 40 mW); NO (5.2 μm, 60 mW); SO_2 (7.3 μm, 40 mW); CO_2 (2.0 μm, 60 mW). The absorption path length is a distance of 30m from the main unit to the auxiliary unit, but the gas does not actually diffuse throughout the entire optical path, so we use the integrated concentration (concentration * gas length). The main unit uses a lens internally to reflect laser light, which is then combined and emitted together. The secondary unit reflects back to the main unit, and the main unit receives the signal through a coaxial reflector.

The modulation signal is sent to the TDLAS laser; controlling a steady change in the current through the laser, the laser will emit light with a steady change in wavelength, and the detector will receive a waveform corresponding to the modulation signal. The system controls the output wavelength of the laser by regulating its current and temperature. Secondly, the detector collects signals and analyzes them to obtain the raw data of the gas concentration multiplied by gas thickness. Finally, the actual smoke plume value is calculated through calibration.

2.1. Instrumentation

A remote monitoring instrument for ship exhaust includes an optical telemetry module and an operational assurance module.

The optical telemetry module is based on TDLAS technology and combined with the transceiver integrated structure scheme, the combined laser beam emitted by the host arrives at the sub-machine and returns in the original way, and the return beam is then focused and detected by the host. The monitoring indicators include CO_2, NO, NO_2, and SO_2, and the absorption spectra of these gases are selected to be relatively strong and free from other gases, and the wavelengths of the lasers are scanned through the absorption peaks of the targets to be measured by controlling the temperature and current of the lasers, to simultaneously invert and derive the concentration of each component.

An operational assurance module is to provide a guarantee for the normal operation and data transmission of the optical telemetry module, including rainproof chassis, industrial air conditioner, microcomputer, 4G router, etc.

2.1.1. Optical Telemetry Module

The optical telemetry module consists of a transceiver-integrated measurement mainframe and a reflector sub-machine. The telemetry host mainly consists of a light source emitter, an air intake chamber, a spectral detector, and an algorithm processing and data transmission module. The light source transmitter is used to emit laser light of a specific wavelength, the spectral detector is used to receive the laser signal reflected from the sub-machine, and the high-frequency second harmonic detection signal is used for measurement to achieve the monitoring of the exhaust plume in the optical path through the change of the light energy. The technical specifications of the optical telemetry module are shown in Table 1.

Table 1. Technical specifications for the optical telemetry modules.

Type	Parameter
Input voltage	DC 24 V, <6 A
Detection gas	NO_2, SO_2, NO, CO_2
Detection distance	30 m
Response time	<10 ms

2.1.2. Operational Assurance Module

1. Chassis

The chassis includes the shell, circuitry, and control switches. The top of the chassis is airtight, the four bottom corners ensure that the temporary water on the ground does not enter the chassis in rainy weather, and the inner edge of the chassis door is inlaid with a ring of sealing rubber to prevent rainwater from penetrating into the chassis. The cabinet is equipped with power supply and control switches of different voltages to meet the power requirements of different instruments.

2. Industrial computer and 4G router

The ICP is the data center of the equipment, with built-in data processing algorithms and acquisition system, which collects the raw data from the optical telemetry module of the ship's exhaust and sends the data to the designated server through the 4G router (Jinan USR lot Technology Limited, Jinan, China). The purpose of the 4G router is to connect the equipment with the Internet of Things and provide a network for the ICP to realize the data remote transmission and the equipment remote debugging.

3. Industrial air conditioner

Enclosure air conditioning was added based on the need for temperature control to ensure proper operation of the equipment outdoors.

- Install a chassis air conditioner on the side wall of the instrument to ensure a constant temperature inside the device;
- Adjust the current value of the temperature control module of the equipment to provide more power for the laser machine TEC to ensure a stable laser temperature;
- Increase the heat circulation inside the chassis to relieve the heat dissipation pressure and increase the roof to further isolate the external heat.

4. Pressure block

To ensure the stability of the optical path of the equipment, pressure blocks are added outside the chassis to prevent the device from moving in strong wind conditions.

5. Sleeve

To reduce the impact of environmental moisture on the work of the internal equipment, while preventing the equipment out of the optical lens condensation on the water droplets, a sleeve is installed at the light emitting position of the equipment.

2.2. Measurement Site

The Zhenjiang section of the Beijing-Hangzhou Canal, with a total length of 42.6 km, is an important part of the Beijing-Hangzhou Canal, which is the main waterway between the north and south of China. The Jianbi locks are located at the crossroads of the Yangtze River and the Beijing-Hangzhou Canal, which is the most convenient and safest water transport channel connecting the southern and northern sections of the Beijing-Hangzhou Canal and is also the only lock in the South Jiangsu Canal that directly reaches the Yangtze River. Its annual cargo volume and the density of ships make it extremely important in the main water transport corridor of the country, as shown in Figure 2.

The equipment was chosen to be installed at the Jianbi locks, the entrance from the Beijing-Hangzhou Canal to the Yangtze River, as shown in the red circle in Figure 2b. The main engine and the secondary engine of the optical telemetry equipment for ship exhaust were fixedly installed on the banks of the two sides of the locks, respectively. The width of the locks is about 24 m, and the height of the equipment from the water surface is about 6–8 m. The location has been cemented and hardened, and facilities such as surveillance

cameras and meteorological monitoring are already in place. The yellow rectangular box indicates the ships waiting in the locks. The area around the measuring station is mainly rural and sparsely populated, with no obvious sources of air pollution. Therefore, the location of the monitoring site is well suited for the detection of nitrogen oxides (NO_x) with relatively low background concentrations.

Figure 2. (**a**) The installation location of telemetry equipment for the Jianbi locks is at the confluence of the Yangtze River and the Beijing-Hangzhou Canal. (**b**) The yellow rectangular box represents the Jianbi locks. (**c**) The on-site photo of the equipment.

2.3. Data Processing

The ship exhaust telemetry equipment measures the concentration data of ship exhaust components entering and leaving the locks in real time, and the data acquisition and processing control unit analyzes and calculates through algorithms to obtain the concentration data of different gas components of ship exhaust. The monitoring curves are drawn with time as the horizontal coordinate and changes in gas concentration of different components as the vertical coordinate.

1. Automatic identification algorithm for ship exhaust gas peaks

The biggest feature of the ship exhaust signal different from the background is the wave peaks of NO and CO_2 synchronously increasing and then decreasing. The ship exhaust wave crest automatic identification algorithm firstly filters and differentiates the telemetry data to give the incremental discrimination index, then combines the time-varying correlation of the NO and CO_2 concentrations for the correlation discrimination index, and finally, synthesizes the two to obtain the comprehensive discrimination index, which is used to identify the wave crests in the time course of the telemetry data of the NO and CO_2 concentrations of the ship exhaust gas. The specific steps are as follows:

Step 1: Obtain data $C_N(t_k)$ and $C_C(t_k)$ ($k = 1, 2, \ldots, N$) of the NO and CO_2 concentrations over time at the monitoring site time T. $t_k = k\Delta t$ is the time series, Δt is the sampling interval, and $N = T/\Delta t$ is the length of the data (taken as an even number).

Step 2: Determine the time scale $T_p = P\Delta t$, and P is the length of data corresponding to the time scale (take an even number). Perform noise reduction filtering on $C_N(t_k)$ according to Equation (7) to obtain $C'_N(t_j)$ ($j = 1, 2, \ldots, N$), with $t_j = j\Delta t$ as the time series.

$$C'_N(t_j) = \sum_{m=1}^{N}\left[\sum_{k=1}^{N}\frac{C_N(t_k)\cdot\exp\left(-2\pi\sqrt{-1}mk/N\right)}{1+\sqrt{-1}mP/N}\right]\cdot\exp(2\pi\sqrt{-1}mj/N) \quad (7)$$

where $m = 1, 2, ..., N$ are discrete sequences.

Step 3: Calculate the NO incremental discriminant $D_N(t_j)$ according to Equation (8).

$$D_N(t_j) = \begin{cases}\left[C'_N(t_{j+1}) + C'_N(t_{j-1}) - 2C'_N(t_j)\right]/\Delta t^2 & 1 < j < N \\ 0 & j = 1 \text{ or } N\end{cases} \quad (8)$$

When $D_N(t_j) < 0$, take $D_N(t_j) = 0$.

Step 4: Calculate the CO_2 and NO correlation discriminant index $R_{CN}(t_j)$ according to Equation (9).

$$R_{CN}(t_j) = \begin{cases}\frac{P\sum_{k\in\delta_{jP}}C_N(t_k)C_C(t_k) - \sum_{k\in\delta_{jP}}C_N(t_k)\sum_{k\in\delta_{jP}}C_C(t_k)}{\sqrt{P\sum_{k\in\delta_{jP}}C_N^2(t_k) - \left[\sum_{k\in\delta_{jP}}C_N(t_k)\right]^2}\sqrt{P\sum_{k\in\delta_{jP}}C_C^2(t_k) - \left[\sum_{k\in\delta_{jP}}C_C(t_k)\right]^2}} & 2 < j < N-1 \\ 0 & \text{otherwise}\end{cases} \quad (9)$$

where $\delta_{jP} = \{k \in \mathbb{Z} | \max(1, j - P/2) \le k \le \min(N, j + P/2)\}$ and moment t_k is in the temporal neighborhood near moment t_j. When $R_{CN}(t_j) < 0$, take $R_{CN}(t_j) = 0$.

Step 5: Calculate the composite discriminant indicator $I(t_j)$ according to Equation (10).

$$I(t_j) = \frac{D_N(t_j)}{\max\limits_{1\le j\le N}\left[D_N(t_j)\right]}\cdot\frac{R_{CN}(t_j)}{\max\limits_{1\le j\le N}\left[R_{CN}(t_j)\right]} \quad (10)$$

Step 6: The wave moments in which the integrated discriminant index $I(t_j)$ exceeds the threshold I_0 and the interval exceeds T_p are recorded as the wave marking moments t_{qi} ($i = 1, 2, \ldots, Q$), Q is the number of identified waves, and q_i is the time sequence number corresponding to the i wave marking moment.

2. Automatic emission factor measurement method

Different from the sniffing method [26–28], the optical method in the hardware to achieve the integration of different gases in the optical path, different lasers emitted to the received light aggregated together to ensure that different lasers measured gas for the same gas, so that the concentration of different indicators of the concentration of the change curve has a very good synchronization. Therefore, the pollutant emission factor can be calculated by using the linear regression of the pollutant and CO_2. The formula of linear regression is as follows:

$$\begin{gathered}a = \frac{\sum xy - \frac{1}{N}\sum x\sum y}{\sum x^2 - \frac{1}{N}(\sum x)^2} \\ b = \overline{y} - a\overline{x}\end{gathered} \quad (11)$$

x and y are arrays of concentration values of pollutant X and CO_2, respectively, over a time range. a is the slope, the multiple by which pollutant X increases as the CO_2 concentration

increases. b is the intercept, the background CO_2 concentration multiplied by a when the pollutant concentration is zero.

Since the CO_2 concentration in the fuel can be assumed to be equal to 87%, the emission factor (EF) for pollutant X is calculated as follows:

$$\mathrm{EFx(g/kg)} = a \times (\text{molecular weight})\ x \times 72.5 \quad (12)$$

In addition, the emission factor for NO_x is the sum of NO and NO_2 and is simply calculated by substituting the molecular weight of NO_2 into Equation (12) when calculating the NO emission factor.

3. Experimental Results and Analysis

Each time the locks are opened, eight ships below Figure 2a (Beijing-Hangzhou Canal) are allowed to enter the waiting area inside the locks and wait for the opening of the locks gate above Figure 2a (Yangtze River). After all the eight ships enter the Yangtze River, the next round of eight ships enters the locks waiting area from above Figure 2b and exit from below Figure 2b after the gate is opened. The above complete process is a cycle (ships below entering the locks → ships exiting from above → ships above entering the locks → ships exiting from below), and the interval between the two cycles is very short; that is, after all the "down-out" ships leave the locks and enter the canal, the "down-in" ships waiting on the canal side of the locks generally begin to enter the locks one by one in less than 10 min.

The telemetry equipment is installed at the entrance of the Beijing Hangzhou Canal at the ship locks, and the monitored objects are "down-in" and "down-out" ships. According to on-site observations, the "down-in" ships entering the locks from the canal are often empty, with shallow draft, and the masts or facilities on top of the ships may block the light path, which is reflected in the large negative value of the monitored concentration. The "down-out" ships entering the locks from the Yangtze River tend to leave fully loaded, with deeper draft, which masts or facilities on top of the vessels generally do not block the light path. Overall, the difference in height between the two types of vessels is about 2 m, and the telemetry results may vary considerably.

3.1. Analysis of Detection Rate for Unloaded and Fully Loaded Vessels

In 2024, a remote experimental test was conducted at the monitoring point of the Jianbi locks, and the telemetry data were analyzed for 45 h, during which, a total of 656 vessels passed by the telemetry point in total, of which 352 were fully loaded vessels and 304 were unloaded vessels. The monitoring instrument telemetered a total of 330 vessels, 255 fully loaded vessels and 75 unloaded vessels, as shown in Figure 3. The detection rate of the vessels was 50.3%, the detection rate of the fully loaded vessels was 72.4%, and that of unloaded vessels was 24.7%, as shown in Table 2.

Table 2. Experimental data.

	Passing Vessels	Telemetry Vessels	Detection Rate
Unloaded vessels	304	75	24.7%
Fully loaded vessels	352	255	72.4%

As can be seen from Table 2, the detection rate of ships was 50.3%, and the remaining ships were not telemetered, probably because (i) the wind direction was parallel to the locks channel, and the wind speed exceeded a certain speed, which prevented the exhaust plume emitted by ships from spreading to the height of the monitoring instrument, and

therefore, the exhaust signal could not be telemetered; (ii) the ship's chimneys exceeded the monitoring height of the telemetry instrument, the exhaust plume emitted by the ship could not spread to the monitoring instrument, and therefore, the exhaust signal could not be telemetered.

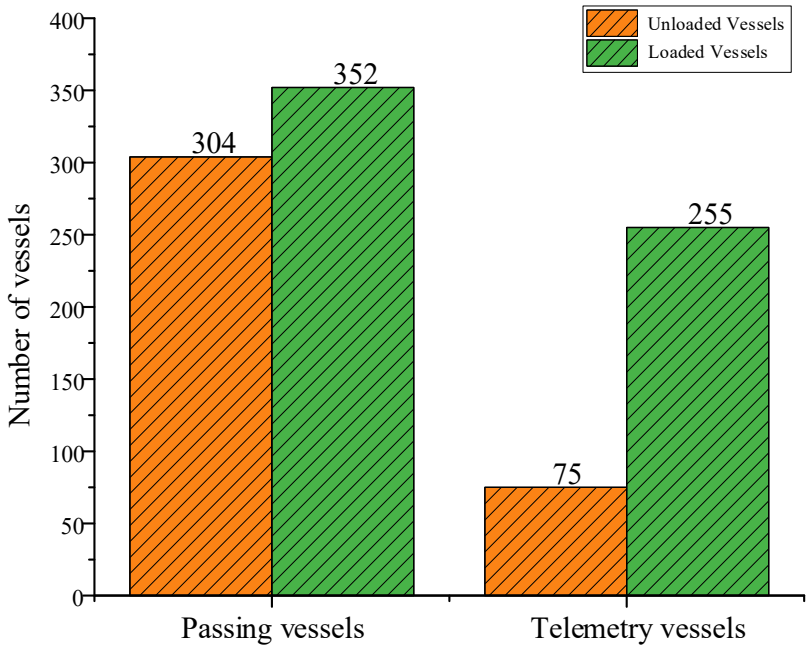

Figure 3. The number of vessels that passed through telemetry stations during the experiment, and the number of vessels which exhaust signals were detected by instruments.

In addition, the detection rate of 72.4% for fully loaded vessels is much higher than the detection rate of 24.7% for unloaded vessels, which may be due to, (i) with the same vessel speed, the more heavily loaded vessel requires more power, i.e., a larger amount of exhaust gas, and it is easy to telemetry the exhaust gas signal, and (ii) the draught depth of unloaded vessels is low, and most of the vessels with exhaust ports beyond the monitoring height of the remote monitoring instrument are unable to measure the exhaust signal.

3.2. Analysis of Exhaust Emission Patterns from Inland Vessels

The monitoring data of 4 h were selected for the experiment, as shown in Figure 4, and it can be found that the 4 h contained three complete cycles of vessels entering and leaving the locks, with every two orange dashed lines representing a complete cycle, so each cycle was about one and a half hours. Among them, it took about 15 min for the fully loaded vessels and about 15 min for the unloaded vessels, with an interval of about 1 h in between. From Figure 4, the masking phenomenon was more serious in the case of the unloaded vessels and less serious in the case of the fully loaded vessels.

As can be seen from Figure 5, the waveform signals of CO_2 and NO_x monitored by the remote monitoring instrument are strong, which can be applied to the regulation of NO_x emissions from inland vessels. From Figure 5, even for the same group of fully loaded vessels, there are some differences in the waveforms of ship exhaust signals. Some of the waveforms are sharp and the signal intensity is high, probably because the chimney is located on the top of the ship, and the telemetry plume is closer to the chimney opening, so the duration is shorter and the concentration is higher. Some of the peaks are wider and the signal intensity is low, probably because the chimney is located at the rear of the ship, and the ship's exhaust slowly diffuses into the optical path from the bottom to the top, resulting in longer durations and lower concentrations, and there may be multiple peaks on the same ship.

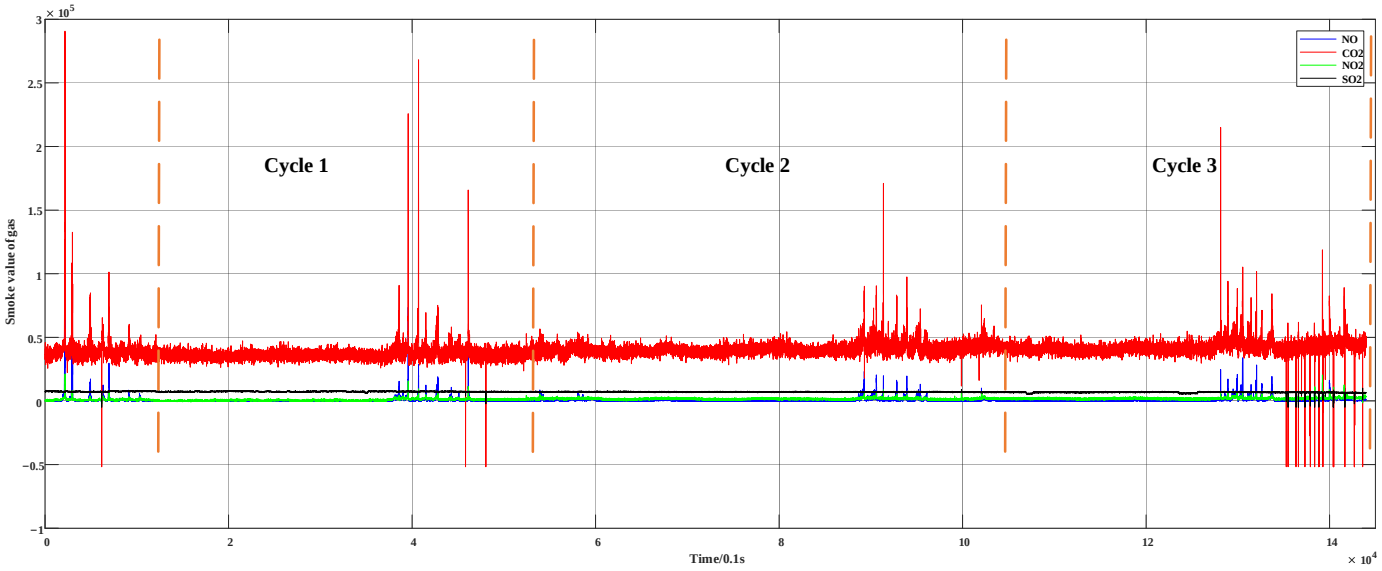

Figure 4. Monitoring results for 4 consecutive hours (red curve for CO_2, blue curve for NO, green curve for NO_2, and black curve for SO_2).

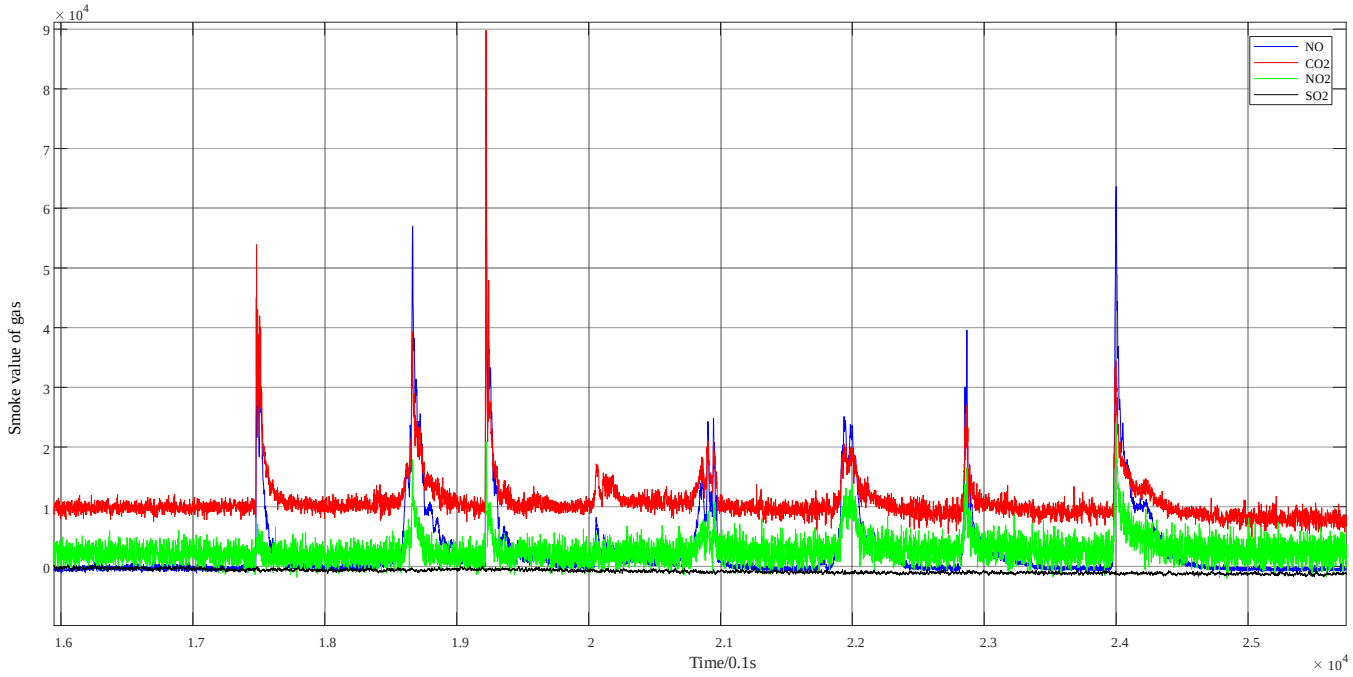

Figure 5. Exhaust monitoring results for a group of eight fully loaded vessels.

Figure 6 illustrates the NO_x and CO_2 linear regression trend plots of the exhaust telemetry results for the eight ships in Figure 6. As can be seen in Figure 6, NO_x has a positive correlation with CO_2, indicating a high degree of synchronization between NO_x and CO_2. In addition, the SO_2 are relatively weak, which cannot be used to regulate whether the fuel sulfur content exceeds the standard for inland vessels using diesel fuel with a sulfur content of 10 ppm (unless it is an extremely serious fuel that exceeds the standard). This demonstrates that the fuel compliance of inland vessels in the Beijing-Hangzhou Canal is relatively high, probably because the fuel supply location is basically on the shore, and the fuel source is consistent with that of diesel trucks; unlike sea vessels along the coast, there may be more high sulfur oils refined by irregular refining enterprises because of the difficulty of regulating the open coastal waters.

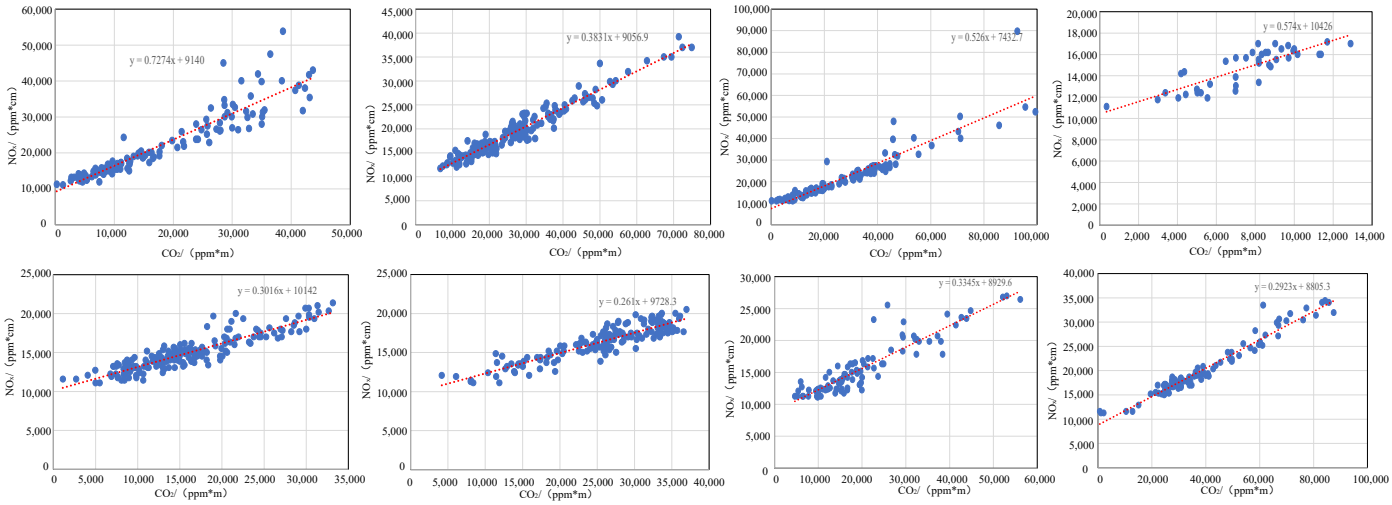

Figure 6. Linear regression trend of NO_x and CO_2 in the ship exhaust.

3.3. Analysis of NO_x Emission Patterns from Unloaded and Fully Loaded Vessels

The results of six cycles of ship exhaust monitoring are presented in Figure 7. The horizontal coordinates represent the time series, the vertical coordinates represent the relative values of the pollutants, the blue curve represents the concentration change curve of NO, and the red curve represents the concentration change curve of NO_2.

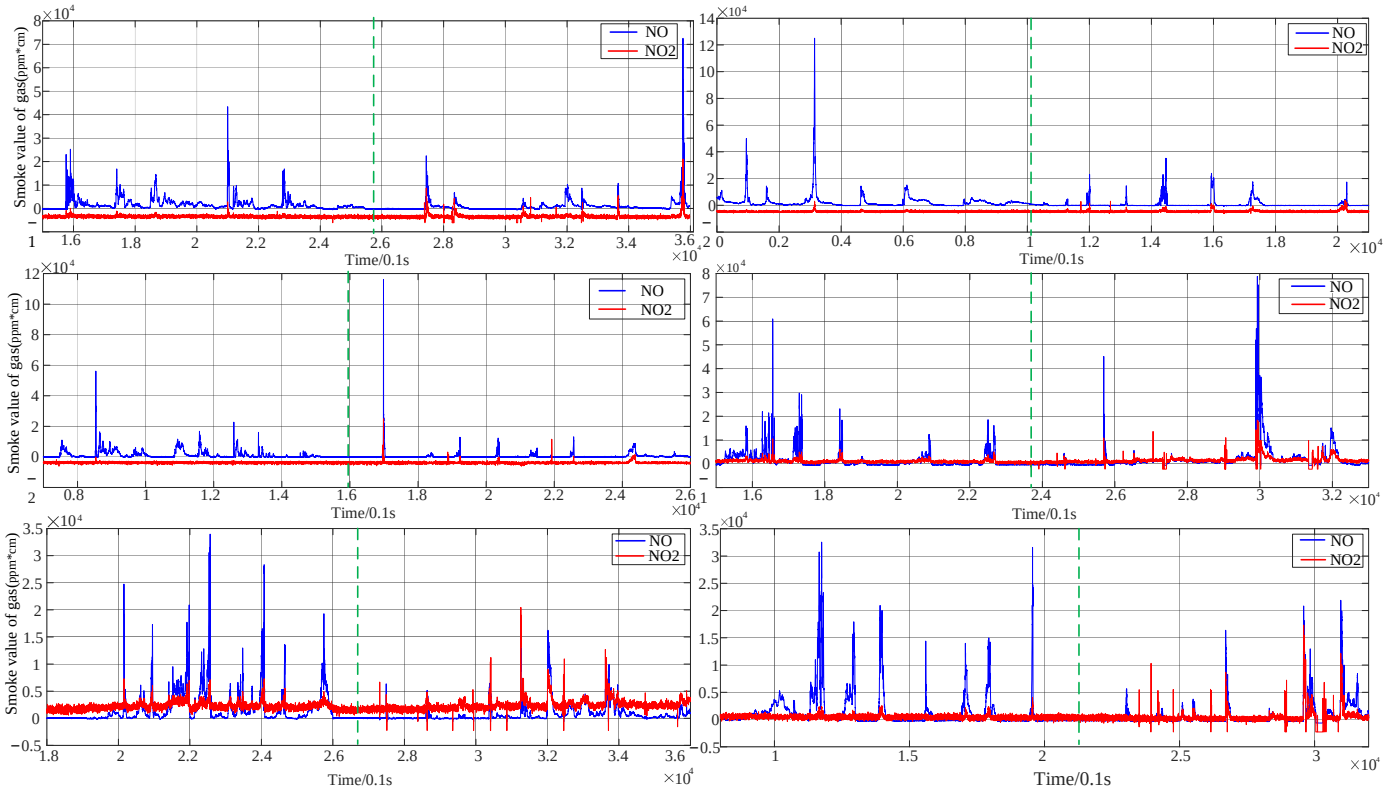

Figure 7. NO_x monitoring results for six groups of fully loaded and unloaded vessels.

The left side of the green dotted line represents the exhaust monitoring curve of the fully loaded vessels (sailing out of the Yangtze River), and the right side of the green dotted line represents the exhaust monitoring curve of the unloaded vessels (sailing into the Yangtze River).

As shown in Figure 7, the NO and NO_2 ratios show that the "down-out" ship has a higher proportion of NO because it is fully loaded and accelerating away and therefore has a higher power (less air combustion in the engine), and the NO concentration is significantly higher than the NO_2 concentration. Compared to the NO_2 concentration of the fully loaded vessels, the "down-in" vessels, because of their unloaded and low speed entry, have less power (The empty combustion in the engine is relatively large.) and a higher proportion of NO_2 (The exhaust gas contains a large concentration of O_2). The experimental results demonstrate that NO_2 must be added to the monitoring indicators of inland vessels; otherwise, there is a serious underestimation of NO_x monitoring results, especially in the case of unloaded vessels.

As shown in Figure 7, the signal intensity of the "down-out" and "down-in" ships are not the same, and there are cases of high signal intensity and low signal intensity. There are two possible reasons for this: one is that the power of the vessels is different and the amount of the exhaust emissions is different, so the exhaust signal intensity is also different. The other is that the location of the ship's exhaust ports is different. There is a certain height difference between the monitoring site and the ship's exhaust port. Vessels with high exhaust port positions are closer to the remote monitoring instrument, so the exhaust signal intensity is higher; on the contrary, ships with low exhaust port positions are further away from the remote monitoring instrument, and after a certain time of diffusion and dilution, the exhaust signal intensity is lower.

3.4. Analysis of Key Parameter of NO_x Emission Factors for Inland Vessels

As mentioned earlier, the experiment monitored a total of 330 vessels, of which 255 were fully loaded vessels and 75 were unloaded vessels. Figure 8a demonstrates the distribution of the key parameter *a* of the NO_x emission factor for the 255 of fully loaded vessels, where the parameter *a* is calculated by Equation (11), and it can be seen from Figure 8a that the key parameter *a* of the NO_x emission factor for most ships is less than 4, and that the key parameter *a* of the NO_x emission factor for a small number of ships is greater than 4. Figure 8b quantifies the statistics of the key parameter *a* of the NO_x emission factor for 255 fully loaded vessels. It can be seen from Figure 8b that, among the 255 fully loaded vessels, 93.7% of the vessels have a key parameter *a* of the NO_x emission factor less than 4, and 6.3% of the vessels have a key parameter *a* of the NO_x emission factor greater than 4. The reason for this difference may be caused by the different heights of the ships' exhaust port positions. Vessels with high exhaust port positions are closer to the remote monitoring instrument, so the exhaust signal waveforms are sharper, i.e., the steeper the rising waveforms are, the greater the key parameter *a* of the NO_x emission factor. On the contrary, vessels with low exhaust port positions are farther away from the remote monitoring instrument, and after a certain time of diffusion and dilution, so the exhaust signal waveform is wider, i.e., the more sloping the rising waveform is, the smaller the key parameter *a* of the NO_x emission factor. In addition, the wind speed and direction will also have some influence on the waveform shape of the telemetry results.

Figure 9a demonstrates the distribution of the NO_x emission factor key parameter *a* for 75 unloaded vessels, from which most of the vessels have a NO_x emission factor key parameter *a* less than 2.5, and a small number of vessels have a NO_x emission factor key parameter *a* greater than 2.5. Figure 9b quantifies the NO_x emission factor key parameter *a* statistics of 75 unloaded vessels, and from Figure 9b, 88% of the 75 unloaded vessels have a NO_x emission factor key parameter *a* less than 2.5, and 12% of the vessels have a NO_x emission factor key parameter *a* greater than 2.5. The reason for the differences may be caused by the high or low position of the ships' exhaust ports and the influence of wind speed and direction.

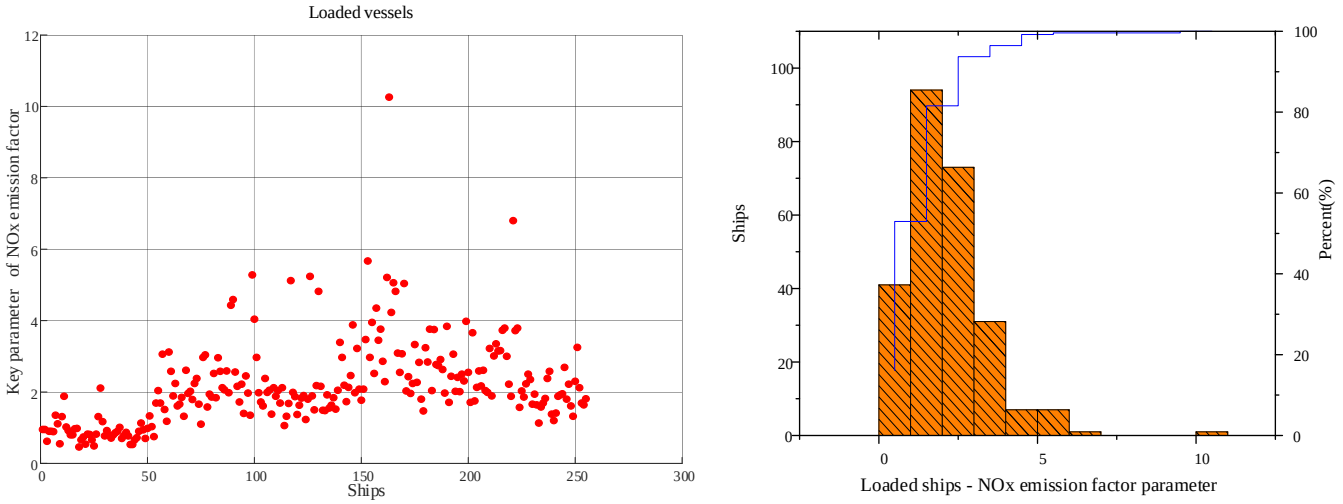

Figure 8. (**a**) Distribution of key parameter *a* of NO_x emission factors for 255 fully loaded vessels. (**b**) Statistics of key parameter *a* of NO_x emission factors for 255 fully loaded vessels.

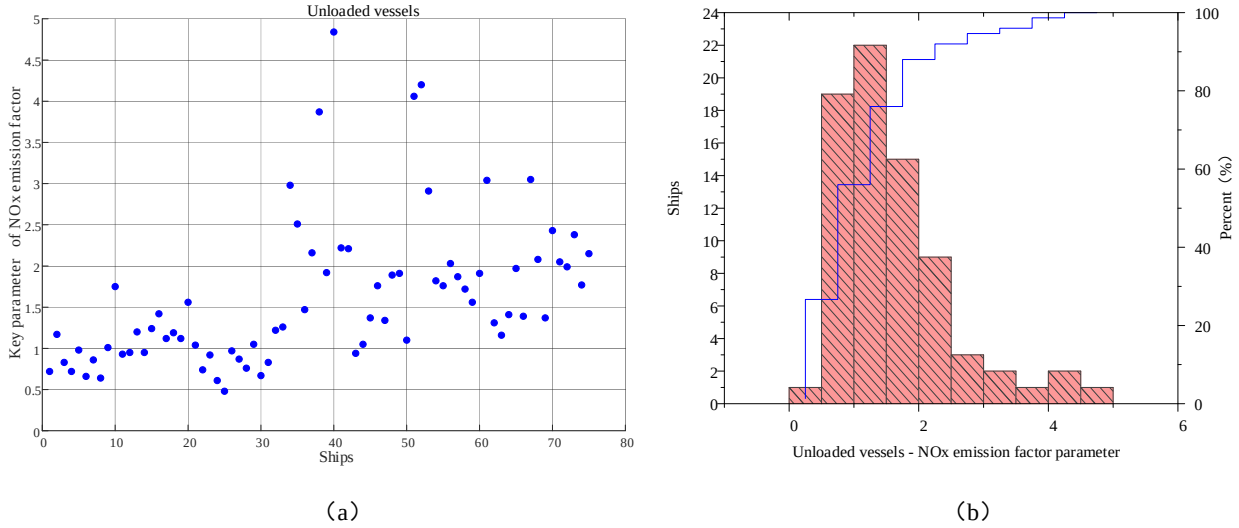

Figure 9. (**a**) Distribution of the key parameter *a* of NO_x emission factors for 75 unloaded vessels. (**b**) Statistics of the key parameter *a* of NO_x emission factors for 75 unloaded vessels.

4. Discussion

This study aims to narrow the research gap by monitoring NO_x emissions from inland vessels based on the TDLAS approach. The main contributions of this study include:

(i) A remote monitoring equipment for inland vessel emissions is designed to monitor the emissions of NO_x, CO_2, and SO_2 in the exhaust of inland vessels entering and exiting the locks in real time.

(ii) Comprehensive analyses were conducted on the tailpipe emission patterns of river vessels, the NO_x emission patterns of fully loaded and unloaded vessels, the detection rate, and the key parameter of the NO_x emission factor of inland vessels.

(iii) The signals of CO_2 and NO_x monitored by the equipment are very strong and well synchronized, which can be applied to the regulation of NO_x emission from inland vessels.

5. Conclusions

In this paper, a remote monitoring equipment for inland vessel emissions based on TDLAS technology is designed to monitor emissions from inland vessels entering and exiting the locks in real time. A total of 330 vessels were monitored in the experiment. The detection rate was 50.3% for vessels, 72.4% for fully loaded vessels, and 24.7% for unloaded vessels. In addition, the exhaust emission pattern of inland vessels, the NO_x emission pattern and detection rate of unloaded and fully loaded vessels, and the key parameter of the NO_x emission factor of inland vessels were comprehensively analyzed.

The experimental results show that the signals of the CO_2 and NO_x emissions from inland vessels are of high intensity and well synchronized, which can be applied to the regulation of NO_x emissions from inland vessels. In addition, NO_2 must be added to the monitoring indicators of inland vessels; otherwise, there is a more serious underestimation of the NO_x results. As a party to Annex VI of the MARPOL Convention, China has completed the domestic legislative procedures for ships on international voyages and realized the effective control of exhaust emissions from ocean-going vessels. However, for ships on domestic voyages, emission standards for common pollutants such as NO_x from domestic marine engines should be formulated and released as soon as possible in light of China's national conditions and aligned with the requirements of Annex VI to realize a substantial reduction in NO_x emissions from ships on domestic voyages.

However, the application of technology in this study still faces many challenges, such as (i) the complexity of inland vessels is much higher than that of diesel vehicles due to the large difference in tonnage, various structural forms, and variable locations of exhaust ports; (ii) depending on the amount of cargo carried by inland vessels (unloaded or fully loaded are the two extreme cases), the height of the vessel's exhaust port from the water surface is different, and there may be a floating space of several meters between the two, so there will be a certain degree of difference in the intensity of the exhaust signal monitored; (iii) the concentration of exhaust gases emitted from fully loaded vessels and unloaded vessels, in which the NO/CO_2 and NO_2/CO_2 ratios are obviously different, ensure the experimental results fully demonstrate that NO_2 must be added to the exhaust telemetry indicators of inland vessels; and (iv) the range in water level changes between mountain locks and plains locks varies greatly. Applying exhaust telemetry technology in the fixed position of the locks, the position of the monitored plume, or even whether the plume can be monitored, is uncertain, which brings about a great challenge to the application of telemetry technology.

Author Contributions: Data curation, M.D. and Z.Q.; Formal analysis, M.D. and S.P.; Funding acquisition, J.H. and Z.Q.; Investigation, M.D. and Z.Q.; Methodology, J.H.; Project administration, S.P.; Supervision, J.H. and S.P.; Validation, J.H.; Visualization; Writing—original draft, M.D. All authors have read and agreed to the published version of the manuscript.

Funding: This research was funded by the National Key Research and Development Program of China (2023YFC3707300) and the National Natural Science Foundation of China (52302435).

Data Availability Statement: The data presented in this study are available on request from the corresponding author. The data are not publicly available due to privacy.

Acknowledgments: The authors thank the staff of Jianbi locks for their support in the process of paper the experiments.

Conflicts of Interest: The authors declare that they have no conflicts of interest.

References

1. International Chamber of Shipping. Impact Of COVID-19 and the Intensifying Crew Change Crisis–ICS 2020 Annual Review. Available online: https://www.ics-shipping.org/publication/annual-review-2020/ (accessed on 10 March 2024).
2. UNCTAD. World Seaborne Trade by Types of Cargo and by Group of Economies, Annual. United Nations Conference on Trade and Development. Available online: https://unctadstat.unctad.org/wds/TableViewer/tableView.aspx?ReportId=32363 (accessed on 5 March 2024).
3. Eyring, V.; Köhler, H.W.; van Aardenne, J.; Lauer, A. Emissions from International Shipping: 1. The last 50 Years. *J. Geophys. Res.* **2005**, *110*, D17305. [CrossRef]
4. Eyring, V.; Isaksen, I.S.A.; Berntsen, T.; Collins, W.J.; Corbett, J.J.; Endresen, O.; Grainger, R.G.; Moldanova, J.; Schlager, H.; Stevenson, D.S. Transport impacts on atmosphere and climate: Shipping. *Atmos. Environ.* **2010**, *44*, 4735–4771. [CrossRef]
5. Lai, H.K.; Tsang, H.; Chau, J.; Lee, C.H.; McGhee, S.M.; Hedley, A.J.; Wong, C.M. Health impact assessment of marine emissions in Pearl River Delta region. *Mar. Pollu. Bull.* **2013**, *66*, 158–163. [CrossRef] [PubMed]
6. Liu, H.; Fu, M.; Jin, X.; Shang, Y.; Shindell, D.; Faluvegi, G.; Shindell, C.; He, K. Health and climate impacts of ocean-going vessels in East Asia. *Nat. Clim. Change* **2016**, *6*, 1037–1041. [CrossRef]
7. Yang, D.; Kwan, S.; Lu, T.; Fu, Q.; Cheng, J.; Streets, D.G.; Wu, Y.; Li, J. An emission inventory of marine vessels in shanghai in 2003. *Environ. Sci. Technol.* **2007**, *41*, 5183–5190. [CrossRef] [PubMed]
8. Lv, Z.; Liu, H.; Ying, Q.; Fu, M.; Meng, Z.; Wang, Y.; Wei, W.; Gong, H.; He, K. Impacts of shipping emissions on $PM_{2.5}$ pollution in China. *Atmos. Chem. Phys.* **2018**, *18*, 15811–15824. [CrossRef]
9. Feng, J.; Zhang, Y.; Li, S. The influence of spatiality on shipping emissions, air quality and potential human exposure in the Yangtze River Delta/Shanghai, China. *Atmos Chem Phys.* **2019**, *19*, 6167–6183. [CrossRef]
10. Feng, S.H.; Barbara, F. International Experience of Low and Zero Emission Policies in Domestic Shipping. Natural Resources Defense Council. Available online: http://www.nrdc.cn/Public/uploads/2020-07-27/5f1e8aeceb6f1.pdf (accessed on 8 February 2024).
11. Carduner, K.R.; Colvin, A.D.; Leong, R.Y.; Schuetzle, D.; Mackay, G.I.; Karecki, D.R.; Schiff, H.I. Application of tunable diode laser spectroscopy to the real-time analysis of engine oil economy. *Environ. Sci. Technol.* **1992**, *26*, 930–934. [CrossRef]
12. Burgard, D.A.; Bria, C.R.M.; Berenbeim, J.A. Remote Sensing of Emissions from In-Use Small Engine Marine Vessels. *Environ. Sci. Technol.* **2011**, *45*, 2894–2901. [CrossRef] [PubMed]
13. Daniel, A.B.; Carmen, R.M.B. Bridge-based sensing of NO_x and SO_2 emissions from ocean-going ships. *Atmos. Environ.* **2016**, *136*, 54–60.
14. Waclawek, J.P.; Lewicki, R.; Jahjah, M.; Ma, Y.; Tittel, F.K. A sensitive CW DFB quantum cascade laser based QEPAS sensor for detection of SO_2. In Proceedings of the 2012 Conference on Lasers and Electro-Optics (CLEO), San Jose, CA, USA, 6–11 May 2012.
15. Hartmann, A.; Strzoda, R.; Schrobenhauser, R.; Weigel, R. CO_2 sensor for mainstream capnography based on TDLAS. *Appl. Phys. B* **2014**, *116*, 1023–1026. [CrossRef]
16. Genner, A.; Pedro, M.-M.; Moser, H.; Lendl, B. A Quantum Cascade Laser-Based Multi-Gas Sensor for Ambient Air Monitoring. *Sensors* **2020**, *20*, 1850. [CrossRef] [PubMed]
17. Mellqvist, J.; Conde, V. D2.2–Prototype of Revised Sniffer Type of Remote Monitor. Chalmers University of Technology. The SCIPPER Project–814893. (pp. 5–6). 2020. Available online: https://www.scipper-project.eu/library/ (accessed on 30 September 2024).
18. Yao, L.; Liu, W.Q.; Liu, J.G.; Kan, R.F.; Xu, Z.Y.; Ruan, J.; Yuan, S. Measurements of CO_2 Concentration Profile in Troposphere Based on Balloon-Borne TDLAS System. *Spectrosc. Spect. Anal.* **2015**, *35*, 2787–2791.
19. Liu, Q.Q.; Zhu, H.L.; Guo, G.Q.; Wang, Z.Y.; Feng, S.L.; Qiu, X.B.; He, Q.S.; Li, C.L. Simultaneous Detection of SO_2 and SO_3 Based on Mid-IR Quantum Cascade Laser System. *J. Atmos. Environ. Opt.* **2021**, *16*, 424–431.
20. Zhang, R.; Wang, B.; Xue, J.B.; Cheng, L.X.; Yu, Y.B. Design of data acquisition system for TDLAS-type CO_2 gas detection based on Zynq. *Laser J.* **2022**, *10*, 30–33.
21. Hinkley, E.D. High-resolution infrared spectroscopy with a tunable diode laser. *Appl. Phys. Lett.* **1970**, *16*, 351–354. [CrossRef]
22. Yi, J.; Namjou, K.; Zahran, Z.N.; Mccann, P.J.; Richter-Addo, G.B. Specific Detection of Gaseous NO and 15NO in the Headspace of Liquid-phase Reactions Involving NO-Generating Organic, Inorganic, and Biochemical Samples Using a Mid-Infrared Laser. *Nitric Oxide* **2006**, *15*, 154–162. [CrossRef]
23. Nagali, V.; Chou, S.I.; Baer, D.S.; Hanson, R.K.; Segall, J. Tunable diode-laser absorption measurements of methane at elevated temperatures. *Appl. Opt.* **1996**, *35*, 4026–4032. [CrossRef]
24. Nelson, D.D.; Zahniser, M.S.; Mcmanus, J.B.; Kolb, C.E.; Jiménez, J.L. A tunable diode laser system for the remote sensing of on-road vehicle emissions. *Appl. Phys. B* **1998**, *67*, 433–441. [CrossRef]
25. Sun, Y.; Han, Y.; Wei, X.; Gao, P. Non-isothermal reduction kinetics of oolitic iron ore in ore/coal mixture. *J. Therm. Anal. Calorim.* **2016**, *123*, 703–715. [CrossRef]

26. Alföldy, B.; Lööv, J.B.; Lagler, F.; Mellqvist, J.; Berg, N.; Beecken, J.; Weststrate, H.; Duyzer, J.; Bencs, L.; Horemans, B.; et al. Measurements of air pollution emission factors for marine transportation in SECA. *Atmos. Meas. Techn. Discuss.* **2013**, *5*, 8925–8967. [CrossRef]
27. Balzani Lööv, J.M.; Alfoldy, B.; Gast, L.F.L.; Hjorth, J.; Lagler, F.; Mellqvist, J.; Beecken, J.; Berg, N.; Duyzer, J.; Westrate, H. Field test of available methods to measure remotely SO_x and NO_x emissions from ships. *Atmos. Meas. Techn.* **2013**, *6*, 9735–9782.
28. Kattner, L.; Mathieu-üffing, B.; Burrows, J.P.; Richter, A.; Schmolke, S.; Seyler, A.; Wittrock, F. Monitoring compliance with sulfur content regulations of shipping fuel by in situ measurements of ship emissions. *Atmos. Chem. Phys.* **2015**, *15*, 11031–11047. [CrossRef]